# Supplemental Materials for Observation of Townes Solitons in a Two-Component Planar Bose Gas

B. Bakkali-Hassani[1], C. Maury[1], Y.-Q. Zou[1], É. Le Cerf[1], R. Saint-Jalm[3], P.C.M. Castilho[2], S. Nascimbene[1], J. Dalibard[1], J. Beugnon[1]
[1]*Laboratoire Kastler Brossel, Collège de France, CNRS, ENS-PSL University, Sorbonne Université, 11 Place Marcelin Berthelot, 75005 Paris, France*
[2]*Instituto de Física de São Carlos, Universidade de São Paulo, CP 369, 13560-970 São Carlos, Brazil and*
[3]*Department of Physics, Ludwig-Maximilians-Universität München, Schellingstr. 4, D-80799 München, Germany*
(Dated: May 5, 2021)

## 1 - RAMAN BEAM SHAPING

We describe the procedure for preparing a two-component gas with a specific spin pattern, as reported in the main text. We start from a homogeneous sample of atoms in state $|1\rangle$ filling a disk-shaped box potential of radius $R = 20\,\mu$m, with a 2D-density defined as $n_\infty$. Atoms are transferred from state $|1\rangle$ to state $|2\rangle$ using a pair of co-propagating Raman beams along the $\hat{z}$-direction, the two beams having the same waist $w \sim 40\,\mu$m. The frequency difference between the two beams is resonant with the hyperfine energy splitting of 6.8 GHz between the two states. In addition, the wavelength of each beam is set to $\lambda \simeq 789.9\,$nm, in between the D1 and D2 lines of $^{87}$Rb. This allows us to cancel the scalar light-shift induced by the Raman beams which could, because of intensity gradients, print a non-uniform phase on the atomic states over the cloud size. The Raman pulse duration is short enough ($< 25\,\mu$s for all data studied in the main text) so that no dynamics occur during the transfer.

Before reaching the atomic plane, the Raman beams reflect on a DMD (DLP7000 from Texas Instruments interfaced by Vialux GmbH) which we use as an intensity modulator to tune the intensity and hence the local Rabi frequency of the Raman beams driving the atomic transition. Despite the fact that such a modulator displays a binary image ("black or white"), we can create a grey-level image on the atoms by averaging the contribution of many pixels over a size of $1\,\mu$m, which corresponds to both our typical optical resolution and the effective pixel size in the atomic plane of the camera used to image the cloud. The protocol to create such spin patterns is based on an iterative algorithm which minimizes the difference between the measured spin distribution and the targeted one and is discussed in more detail in Ref. [1].

## 2 - EFFECTIVE SINGLE-COMPONENT DESCRIPTION

We present the derivation of an effective single-component description of our two-component system, focusing on the ground state wavefunction. The atomic mixture is described by two coupled non-linear Schrödinger equations (NLSEs)

$$\tilde{\mu}_1\phi_1 = -\frac{1}{2}\nabla^2\phi_1 + (\tilde{g}_{11}n_1 + \tilde{g}_{12}n_2)\phi_1, \tag{1}$$

$$\tilde{\mu}_2\phi_2 = -\frac{1}{2}\nabla^2\phi_2 + (\tilde{g}_{12}n_1 + \tilde{g}_{22}n_2)\phi_2, \tag{2}$$

where $n_i$ is the atomic density for the spin state $i$. We also introduce the reduced chemical potentials $\tilde{\mu}_i = m\mu_i/\hbar^2$. We are interested in localized wavefunctions for the component $|2\rangle$ immersed in a bath of atoms in state $|1\rangle$ extending to infinity. Therefore, the chemical potential $\mu_1$ for the component $|1\rangle$ equals the mean field energy shift $g_{11}n_\infty$ at the asymptotic density $n_\infty$.

The effective single-component description relies on the vicinity of the interaction coupling constants, i.e.

$$\frac{|\tilde{g}_{12} - \tilde{g}_{11}|}{\tilde{g}_{11}}, \quad \frac{|\tilde{g}_{22} - \tilde{g}_{11}|}{\tilde{g}_{11}} \ll 1, \tag{3}$$

which allows one to simplify the NLSE at lowest order in these small parameters. In this situation, we expect the low-energy dynamics to be dominated by spin waves, such that the total density $n_1 + n_2 = n_\infty + \delta n$ is weakly perturbed, with an excess density $\delta n$ satisfying $|\delta n| \ll n_\infty$. At low energy, the relevant spatial variations occur on the scale of the spin healing length [2], which largely exceeds the bath healing length $\xi = 1/\sqrt{\tilde{g}_{11}n_\infty}$. Therefore, the Laplacian operator can itself be considered of order one in the small parameters defined in Eq. (3), such that the term $\nabla^2\phi_1$ in Eq. (1) can be replaced, at order one, by $\nabla^2\sqrt{n_\infty - n_2}$ (assuming a real-valued wavefunction). This approximation allows one to express the excess density $\delta n$ in terms of the second component only, as

$$\tilde{g}_{11}\delta n = \frac{\nabla^2\sqrt{n_\infty - n_2}}{2\sqrt{n_\infty - n_2}} + (\tilde{g}_{11} - \tilde{g}_{12})n_2. \tag{4}$$

Inserting this expression in Eq. (2), we obtain an effective single-component equation for component $|2\rangle$. As we focus only on component $|2\rangle$ hereafter, we drop the index 2 ($\phi_2, n_2, \tilde{\mu}_2 \to \phi, n, \tilde{\mu}$) and write the effective equation

$$\tilde{\mu}\phi = \tilde{g}_{12}n_\infty\phi - \frac{1}{2}\nabla^2\phi + \tilde{g}_e n\phi + \frac{\nabla^2\sqrt{n_\infty - n}}{2\sqrt{n_\infty - n}}\phi, \tag{5}$$

where we introduce the effective coupling constant

$$\tilde{g}_e = \tilde{g}_{22} - \frac{\tilde{g}_{12}^2}{\tilde{g}_{11}}. \tag{6}$$

The term $\tilde{g}_{12} n_\infty \phi$ corresponds to the interaction energy cost for adding a single particle of component $|2\rangle$ into the bath. Such a global energy shift plays no role in the following, and we absorb it in the chemical potential hereafter. Eq. (5) is a non-linear Schrödinger equation with two non-linear terms. The term $\tilde{g}_e n \phi$ is a standard cubic nonlinearity, corresponding to an effective system of bosonic particles with contact interactions and coupling constant $\tilde{g}_e$ [3]. The second term is more complex and plays a significant role when the density $n$ becomes comparable to the asymptotic bath density $n_\infty$. To be more precise, one can expand, in the limit of large bath density, Eq. (5) in powers of the depletion $n/n_\infty$. At minimal order we obtain the NLSE used in the main text

$$\tilde{\mu}\phi = -\frac{1}{2}\nabla^2\phi + \tilde{g}_e n \phi, \tag{7}$$

with the coupling constant $\tilde{g}_e$.

In the case $\tilde{g}_e < 0$ relevant for our experiments, this equation has, for each negative value of the chemical potential, a localized stationary solution – the so-called Townes soliton – that can be written as

$$\phi_\ell(r) = \frac{1}{\ell\sqrt{G_T}} R(r/\ell), \tag{8}$$

where we introduce the length $\ell = 1/\sqrt{|\tilde{\mu}|}$ and $R$ is the zero-node solution of the differential equation

$$\left(\frac{1}{2}\nabla^2 + R^2 - 1\right) R = 0. \tag{9}$$

This function is normalized to the value $G_T = \int \mathrm{d}^2 r\, R^2(r) \simeq 5.850$. The wave functions $\phi_\ell(r)$ correspond to zero-energy states that have the same atom number, equal to

$$N = N_T = \frac{G_T}{|\tilde{g}_e|}. \tag{10}$$

The self-similar nature of this family of solutions reflects the scale invariance of the NLSE in two dimensions given in Eq. (7).

At next order in the perturbation, we obtain the equation

$$\tilde{\mu}\phi = -\frac{1}{2}\nabla^2\phi + \tilde{g}_e n\phi - \frac{\nabla^2 n}{4n_\infty}\phi. \tag{11}$$

The additional term, which was considered in [4], can be viewed as a weakly non-local interaction. Since it involves an explicit length scale $1/\sqrt{n_\infty}$, it breaks scale invariance, and we no longer expect self-similarity between stationary states. In a linear perturbative treatment, the stationary state is written as a weakly deformed Townes soliton

$$\phi(r) \propto \frac{1}{\ell} R(r/\ell) + \frac{1}{2n_\infty \ell^3} R_2(r/\ell), \tag{12}$$

where $R$ is defined in Eq. (9) and $R_2$ is the solution of

$$\left(\frac{1}{2}\nabla^2 + 3R^2 - 1\right) R_2 = -\frac{1}{2} R\, \nabla^2 R^2. \tag{13}$$

The atom number contained in the perturbed state is always larger than $N_T$ and is pertubatively given by

$$N \simeq N_T \left(1 + 0.23 \frac{N_T}{n_\infty \ell^2}\right). \tag{14}$$

This prediction is in good agreement with the results of numerical simulations described in the following Section.

## 3 - BEYOND THE WEAK DEPLETION LIMIT: SIMULATIONS

We explore here the ground-state properties of our two-component system beyond the weak depletion regime. We compare the different approaches introduced in Section 2 of these Supplemental materials:

- The two coupled NLSEs given by Eqs. (1)-(2).
- The single component effective equation given in Eq.(5), valid for arbitrary depletion and close $g_{ij}$'s.
- The low depletion limit of the previous equation given by Eq. (11) including the first order correction to the scale invariant attractive NLSE.

We show in Fig. 1(a) how the ground state atom number varies with respect to $N_T$ when increasing the depletion for these three models. We also show the analytical prediction of Eq. (14) that we rewrite as

$$N/N_T = 1 + 0.27\,\epsilon. \tag{15}$$

We have introduced the depletion parameter

$$\epsilon = \frac{N_T/\sigma^2}{n_\infty}, \tag{16}$$

with $\sigma$ the rms size of the corresponding state, which is related to the length $\ell$ as $\sigma \simeq 1.09\,\ell$ for the Townes profile of Eq. (8). This quantity can be viewed as the ratio between the typical peak density $N_T/\sigma^2$ in the impurity component $|2\rangle$ and the atom density $n_\infty$ in the bath component $|1\rangle$. All models predict a similar shift of the ground state atom number for values of $\epsilon \lesssim 0.25$, which is the maximum value of all data presented in the main text. We also note that the single component effective model gives a faithful description of the two-component

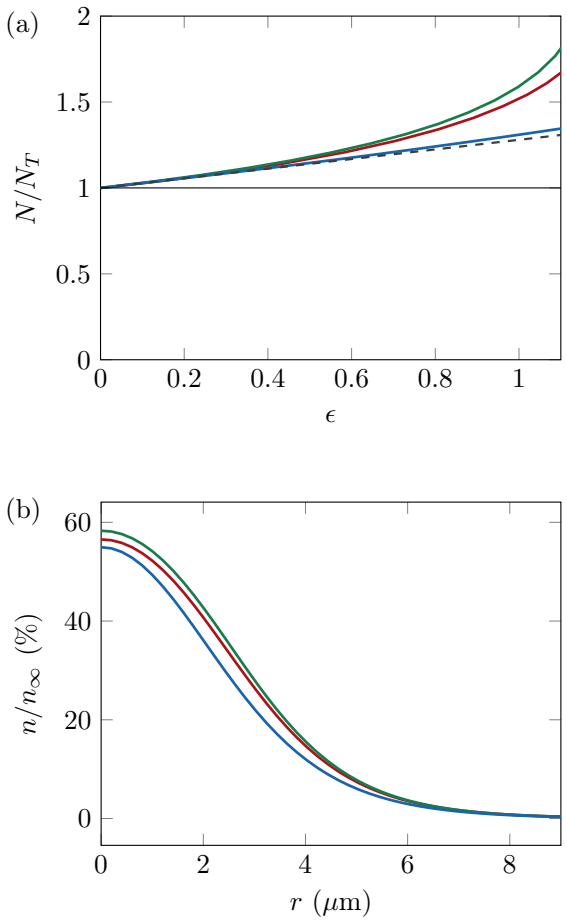


FIG. 1. Numerical study of the ground state for different models. (a) Deviation of the ground state atom number $N$ with respect to $N_T$ as a function of the depletion parameter $\epsilon$ for different models: two-component NLSE (red) with $\tilde{g}_{11} = 0.16$ and $(\tilde{g}_{12}, \tilde{g}_{22}) = (0.98, 0.94)\,\tilde{g}_{11}$, effective one-component NLSE (green), weak depletion expansion of the effective one-component NLSE (blue), analytical prediction of Eq. (15) (dashed black). (b) Radial profiles for $\epsilon = 1$ and $n_\infty = 100\,\mu\text{m}^{-2}$ for the three models with the same color code.

system for both the ground state atom number and the density profile showed in Fig. 1b.

It is interesting to note that our work at small and intermediate depletions connects in the limit of full-depletion of the bath ($n \to n_\infty$ at the center of the bubble) to the physics of spin domains in an immiscible mixture, a situation in which the single-component effective equation introduced in this work may be of interest.

## 4 - EXPERIMENTAL DETERMINATION OF THE RMS SIZE

The results presented in the main text exploit the measured rms size $\sigma^2$ defined as

$$\sigma^2 = \frac{1}{N}\int \mathrm{d}^2 r\, n(\mathbf{r})\, r^2 - \langle \mathbf{r} \rangle^2, \tag{17}$$

where $n$ is the atomic density in state $|2\rangle$. Direct determination of the rms size is challenging experimentally. Indeed, the contribution of the points at large $r$ is important for a 2D integral and our signal to noise ratio is poor in this region. Consequently, we use a fit to the data to determine the rms size. We detail below the choice of the fitting function and the fitting procedure. We confirmed the validity of this method by applying it to the results of numerical simulations of the two-component NLSEs.

*Determination of the fitting function.* We use time-dependent perturbation theory to extract a suitable fitting function for the deformation of the density profile. We consider the evolution of a wave function $\phi$ under the time-dependent NLSE

$$\mathrm{i}\frac{\partial \phi}{\partial \tau} = -\frac{1}{2}\nabla^2 \phi - G|\phi|^2 \phi, \tag{18}$$

with $\tau = (m/\hbar)t$. From Section 2, we know that for $G = G_T$, the stationary solution of Eq. (18) with chemical potential $\tilde{\mu} < 0$ is given by

$$\phi(r, \tau) = \phi_\ell(r) e^{-\mathrm{i}\tilde{\mu}\tau}, \tag{19}$$

with $\ell = 1/\sqrt{|\tilde{\mu}|}$. We consider a wave function $\phi$ given by a Townes profile $\phi_\ell(r)$ at $\tau = 0$, with an interaction parameter $G$ that is slightly different from $G_T$. We define the small parameter of the expansion $\eta$ such that $G = (1 + \eta)G_T$. At short times, the deformation of the wave function with respect to the Townes profile is expected to be small, and we can expand the solution with respect to $\eta$:

$$\phi(r, \tau) = [\phi_\ell(r) + \eta\epsilon(r, \tau) + \ldots] e^{-\mathrm{i}\tilde{\mu}\tau}. \tag{20}$$

We restrict here to the first-order correction in $\eta$, and consider the first terms of the Taylor expansion of $\epsilon(r, \tau)$ with respect to $\tau$:

$$\epsilon(r, \tau) = \epsilon_0(r) + \epsilon_1(r)\tau + \epsilon_2(r)\tau^2 + \ldots \tag{21}$$

The initial condition gives directly $\epsilon_0(r) = 0$, and by injecting the expansion given in Eq. (21) in Eq. (18), we identify

$$\begin{aligned} \epsilon_1(r) &= \mathrm{i}\phi_\ell^3(r) \\ \epsilon_2(r) &= \frac{G_T}{2}\left(-\tilde{\mu} - \frac{1}{2}\nabla^2 - G_T\phi_\ell^2\right)\phi_\ell^3. \end{aligned} \tag{22}$$

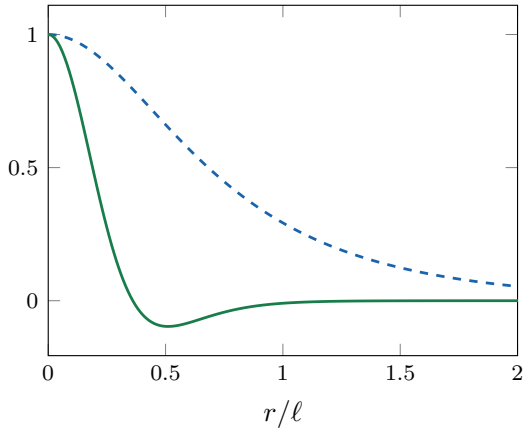


FIG. 2. Townes profile $\phi_\ell(r)/\phi_\ell(0)$ (blue dashed line) and $\chi(r)/\chi(0)$ (green solid line) deduced from perturbation theory and expressed in Eq. (24).

Interestingly, this last identity can be further simplified using Eq. (9) and we obtain

$$\epsilon_2(r) = G_T\left(G_T\phi_\ell^5 + \tilde{\mu}\phi_\ell^3 - \frac{3}{2}\phi_\ell{\phi'_\ell}^2\right). \qquad (23)$$

Related approches were introduced in Refs. [5, 6]. More precisely, the authors of Ref. [6] studied the elementary excitations of the NLSE given in Eq. (18) and looked for exact solutions that were at most polynomials on $t$, while here we do not impose such a constraint but restrict to a short time expansion.

When computing the density profile $n(r,t) = |\phi(r,t)|^2$, only the real term $\epsilon_2$ contributes at first order in $\eta$ (the imaginary term $\epsilon_1$ contributes to the phase of the wavefunction). We deduce the expected deformation of the density profile at first order and at short times

$$\begin{aligned}\delta n(r,t) &= n(r,t) - n(r,0)\\ &\simeq 2\eta\phi_\ell(r)\epsilon_2(r)t^2 \equiv \eta\chi(r)t^2, \qquad (24)\end{aligned}$$

where we have defined $\chi(r) = 2\phi_\ell(r)\epsilon_2(r)$. We checked that the 2D integral of $\chi$ is zero, as the norm of $\phi$ should be conserved by the evolution under Eq. (18). In Fig. 2 we show the profiles $\phi_\ell(r)$ and $\chi(r)$.

*Fitting procedure.* The first step of the data analysis consists in obtaining averaged 1D radial density profiles $n(r,t)$. The averaging is performed after recentering the individual images. Indeed, we observe random drifts of the wave packet from one shot to another, which we attribute to thermal fluctuations.

In a second step, we fit the initial profile to a Townes density profile with a free amplitude and size, which we denote $n^0(r)$. For each time of the evolution we compute the deformation of the density profile with respect to the fitted initial one

$$\delta n(r,t) = n(r,t) - \beta n^0(r), \qquad (25)$$

where $\beta$ is a correction factor to make the two terms of the right-hand-side of Eq. (25) have the same atom number.

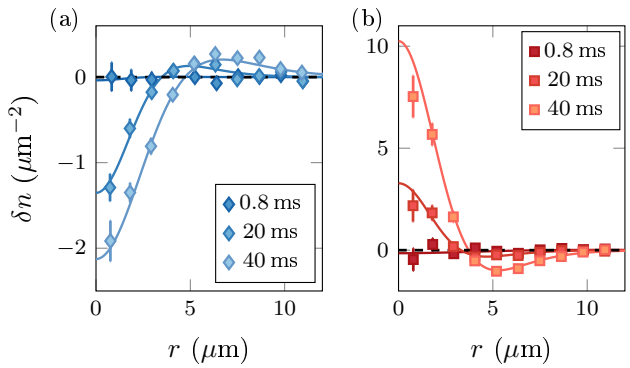


FIG. 3. Difference $\delta n(r,t)$ as defined in equation (25), for various times $t$ of the experimental runs presented in Fig. 2a ($N = 250$) (a) and Fig. 2c ($N = 1200$) (b) of the main text. We also plot the best fit of $\chi(r)$ to the data.

The last step consists in fitting this profile with the function $\chi(r)$ determined in Eq. (24) with a free amplitude and size. This fit is performed on a radial region that extends from 0 to 1.75 $\sigma_0$, with $\sigma_0$ the initial rms size (obtained from the Townes fit). Examples of such fits are reported in Fig. 3. We compute $\sigma$ using this fitting function over the full plane. Additionally, we estimate the error on $\sigma$ by performing a bootstrap analysis.

It is interesting to note that we observe in Fig. 2a of the main text an important variation of the central density $n_0(t)$ (divided by more than a factor 2 in 40 ms) while the signal in the wings varies little and the evolution of the rms size remains small (from $\sim$6 $\mu$m to $\sim$7 $\mu$m). These two observations, which could be surprising are first sight, are nevertheless fully compatible with the time evolution of a Townes-shaped wave packet with a conserved atom number. To illustrate these points, we show in Fig. 4 the simulated time evolution of a single-component attractive Bose gas with $\tilde{g} = 0.0077$, an atom number $N$=250 and an initial rms size $\sigma_0 = 5.8\,\mu$m, similar to the experimental parameters of Fig. 2a in the main text. The density profile in linear scale shown in Fig. 4a qualitatively confirms the decrease of the central density. We also see that a small increase of the density in the wings (more visible in semilog scale in Fig. 4b) is enough to keep constant the area of the profile, which is given in 2D by $2\pi\int n(r)rdr$. Finally, Fig. 4c also confirms the moderate increase of the rms size observed in the experiments. This is specific to the studied profile. For instance, for a 2D Gaussian profile of rms size $\sigma$,

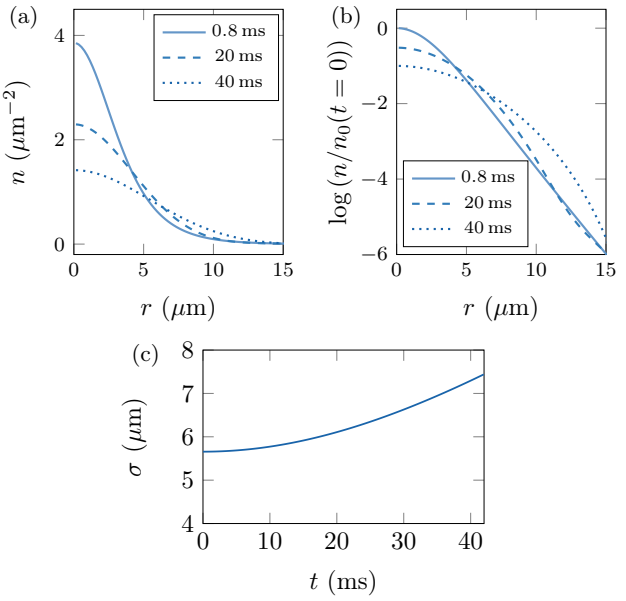


FIG. 4. Time evolution under the NLSE of an attractive Bose gas of 250 particles with an initial size $\sigma_0 = 5.8\,\mu$m. The density distribution in linear (a) and semilog (b) scale and the rms size (c) are shown.

one would expect $n_0\sigma^2$ to be constant during the time evolution and thus an increase of $\sigma$ by a factor $\sqrt{2}$.

## 5 - CONTROL OF THE CRITICAL ATOM NUMBER

We studied in Ref. [7] the dependence of $a_{12}$ with the orientation of the quantization axis given by the magnetic field $\mathbf{B}$. More precisely, if we denote $\Theta$ the angle between $\mathbf{B}$ and the vertical (strongly confining-)axis $\hat{z}$, we can model the 2D inter-component interactions with a dimensionless parameter $\tilde{g}_{12} = \sqrt{8\pi}a_{12}/\ell_z$ where the effective scattering-length has to be corrected from the bare (3D-)value $a_{12}^0 = 98.9\,a_0$, such that

$$a_{12} = a_{12}^0 + \delta a_{12} \quad \delta a_{12} = a_{dd}\left(3\cos^2\Theta - 1\right), \qquad (26)$$

where $a_{dd} = \mu_0\mu_B^2 m/(12\pi\hbar^2) = 0.7\,a_0$ is the dipole length. Despite the smallness of this shift compared to $a_{12}^0$, it has a strong influence on the effective critical atom number $N_T = G_T/|\tilde{g}_e|$, which varies from $N_T(\Theta = 0°) \sim 750$ to $N_T(\Theta = 90°) \sim 5000$ with our experimental parameters. In Fig. 5, we report our measurements of the expansion coefficient $\gamma(N)$ for different orientations $\Theta$ of the magnetic field. We restrict ourselves to $N < 2200$ to ensure the bath stays in the weak depletion limit for the sizes $\sigma \lesssim 9\,\mu$m imposed by the geometry of the experiment. From a linear fit of $\gamma$, with $\gamma(N = 0) = 1.19$ fixed at the expected value, we deduce the stationary atom number $N_T^{\rm exp}(\Theta)$ at which this expansion coefficient vanishes, which is shown in the inset of Fig. 3 of the main text.

Anisotropic effects due to magnetic dipole-dipole interactions are not expected to modify the properties of the system as long as $\sigma \gg \ell_z$, where $\ell_z$ is the vertical confinement length [7]. We checked that the modification of $N_T$ should remain smaller than 5% for all data presented here.

## 6 - UNIVERSAL PROPERTIES OF 2D ATTRACTIVE BOSONS

In Ref. [8], the authors studied the ground state properties of weakly interacting bosons in two dimensions using a classical field formalism with a regularized contact potential. In the following, we recall their main results and show that the expected corrections in our experimental situation are not observable.

One considers bosons in two dimensions interacting via an attractive contact potential $(\hbar^2/m)\tilde{g}\,\delta(\mathbf{r})$, with a dimensionless coupling constant $\tilde{g} < 0$. The quantum treatment of the collisions is mathematically ill-defined for such a contact potential. For $|\tilde{g}| \ll 1$, a more accurate description of the system can be obtained by substituting the bare parameter $\tilde{g}$ by a running coupling constant defined by

$$\frac{1}{\tilde{g}(k)} = \frac{1}{\tilde{g}} + \frac{1}{2\pi}\ln\left(\frac{k_c}{k}\right), \qquad (27)$$

which depends on the relative momentum $k$ of the two particles involved in the collision. The introduction of a cut-off in momentum space $k_c$ is a signature of an intrinsic length scale $1/k_c$ of the physical system given by the van der Waals length scale $R_{\rm vdW} \approx 5\,$nm for $^{87}$Rb. The ground state properties of the system are derived using a variational approach. Here, one considers trial wave functions with a Townes profile of extension $\ell$. The energy per particle of the classical field with $N$ atoms then writes

$$E_N(\ell) \propto \frac{1}{\ell^2} + C\frac{\tilde{g}(\ell^{-1})N}{\ell^2}, \qquad (28)$$

where $C > 0$ is a numerical factor and $\tilde{g}(k)$ is evaluated at the typical momentum $\ell^{-1}$.

In contrast to Eq. (2) of the main text, $E_N$ has now a non trivial dependence on $\ell$ because of the non-constant parameter $\tilde{g}(\ell^{-1})$. This term breaks scale invariance and gives rise to an equilibrium size and a binding energy $(\ell_N, E_N)$ that follow a geometrical law

$$\ell_{N+1} \sim 0.34\,\ell_N \qquad E_{N+1} \sim \frac{1}{(0.34)^2}E_N. \qquad (29)$$

Note that $\ell_N$ and $E_N$ vary extremely rapidly with $N$. For example, one can rewrite $\ell_N$ as

$$\ell_N \sim R_{\rm vdW}\exp\left[-\zeta(N - N_T)\right], \qquad (30)$$

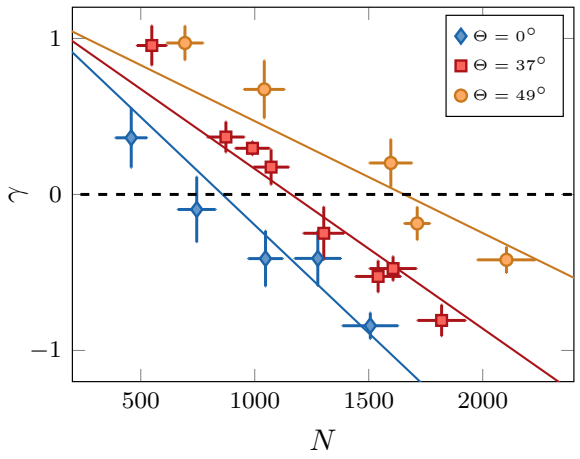


FIG. 5. Expansion coefficient $\gamma$ as a function of the atom number $N$ for varied orientations $\Theta$ of the magnetic field. The rms size of the imprinted cloud is set to $\sigma = 8.6\,\mu$m for all data considered here, and the bath density is $n_\infty = 90$ atom/$\mu$m$^2$. For each set of points we also plot the linear fit of $\gamma(N)$ from which we deduce $N_T^{\rm exp}$.

with $\zeta \approx 1$. For $N = N_T = G_T/|\tilde{g}|$, this size is $\sim R_{\rm vdW}$, which is 3 orders of magnitude smaller than the size of our system. A small shift of only a few atoms, typically from $N_T$ to $N_* \equiv N_T - 6$, gives a size of $\approx$ few microns, compatible with the extension of our system. Experimentally, we cannot resolve the difference between these two atom numbers, as it would require single-particle resolution. Going further away from $N_T$, the corresponding sizes are either much too large or much too small to be experimentally relevant. For this reason, we do not expect to observe a stable state for atom numbers differing significantly from $N_T$ on our experiment.

Finally, we remark that the breakdown of scale-invariance close to $N_*$ is too weak to be observed with our experimental setup. Indeed, consider a system with $N = N_*$ atoms. At equilibrium, Hammer & Son [8] predict an energy per particle $E_{N_*}(\ell_*) \sim -\hbar^2/(N_* m \ell_*^2)$, which is $1/N_*$ smaller than the usual energy associated with the length scale $\ell_* \equiv \ell_{N_*}$. Therefore, if the system is prepared in a Townes profile of size $\ell$ slightly differing from $\ell_*$, the typical energy scale governing the dynamics is

$$E_{N_*}(\ell) - E_{N_*}(\ell_*) \sim \frac{1}{N_T}\frac{\Delta\ell}{\ell_*}\frac{\hbar^2}{m\ell_*^2}, \tag{31}$$

with $\Delta\ell = \ell - \ell_*$. This energy difference $\propto 1/N_T = |\tilde{g}|/G_T$ is thus negligible for $\tilde{g} \ll 1$ and the typical time scale considered in this work.


[1] Y.-Q. Zou, É.. L. Cerf, B. Bakkali-Hassani, C. Maury, G. Chauveau, P. Castilho, R. Saint-Jalm, S. Nascimbene, J. Dalibard, and J. Beugnon, Optical control of the density and spin spatial profiles of a planar Bose gas, arXiv:2102.05492 (2021).

[2] E. Timmermans, Phase separation of Bose-Einstein condensates, Phys. Rev. Lett. **81**, 5718 (1998).

[3] C. Pethick and H. Smith, *Bose–Einstein condensation in dilute gases* (Cambridge university press, 2008).

[4] N. Rosanov, A. Vladimirov, D. Skryabin, and W. Firth, Internal oscillations of solitons in two-dimensional NLS equation with nonlocal nonlinearity, Phys. Lett. A **293**, 45 (2002).

[5] V. Zakharov, Instability of self-focusing of light, Sov. Phys. JETP **26**, 994 (1968).

[6] V. Malkin and E. Shapiro, Elementary excitations for solitons of the nonlinear Schrödinger equation, Physica D: Nonlinear Phenomena **53**, 25 (1991).

[7] Y.-Q. Zou, B. Bakkali-Hassani, C. Maury, E. Le Cerf, S. Nascimbene, J. Dalibard, and J. Beugnon, Magnetic dipolar interaction between hyperfine clock states in a planar alkali Bose gas, Phys. Rev. Lett. **125**, 233604 (2020).

[8] H.-W. Hammer and D. Son, Universal properties of two-dimensional boson droplets, Phys. Rev. Lett. **93**, 250408 (2004).